electronics

Article

Physical Layer Security Performance Analysis of IRS-Aided Cognitive Radio Networks

Zhangyu Liu [1,2], Ji Wang [3], Hao Jiang [4], Jun Wang [5], Xingwang Li [6] and Wenwu Xie [2,7,*]

1 School of Electrical and Electronic Engineering, University Sains Malaysia, Gelugor 11800, Penang, Malaysia; liuzhangyu030@student.usm.my
2 Hunan Hinar Electric Co. Ltd., Yueyang 414006, China
3 College of Physical Science and Technology, Central China Normal University Hubei, Wuhan 430079, China; jiwang@ccnu.edu.cn
4 School of Future Technology, College of Artificial Intelligence, Nanjing University of Information Science and Technology, Nanjing 210044, China; jianghao@nuist.edu.cn
5 CICT Mobile Communication Technology Co., Ltd., Wuhan 430079, China; jwang@cictmobile.com
6 School of Physics and Electronic Information Engineering, Henan Polytechnic University, Jiaozuo 454099, China; lixingwang@hpu.edu.cn
7 School of Information Science and Engineering, Hunan Institute of Science and Technology, Yueyang 414006, China
* Correspondence: gavinxie@hnist.edu.cn

Abstract: Cognitive radio (CR) acts as a significant player in enhancing the spectral efficiency (SE) of wireless telecommunications; simultaneously, the intelligent reflecting surface (IRS) technique is a valid technique for increasing the confidentiality properties of wireless telecommunications systems through the modulation of the amplitude and phase shift of the channel. Therefore, we take into consideration an IRS-assisted multiple-input single-output (MISO) CR system to raise the confidentiality rate, which is composed of a primary network with a primary receiver (PR) and an eavesdropping link, as well as a secondary network with a secondary receiver (SR) and SR transmitter (SR-TX). In particular, we minimize the SR's transmit power under the interference temperature (IT) and confidentiality capacity constraints via the joint optimization of the beamforming vector and artificial noise (AN) constraint matrix at SR-TX together with the phase shift matrix of IRS. Numerical outcomes indicate that various transmit antenna values and the IRS element numbers at SR-TX can greatly reduce transmit power while assuring secure communication.

Keywords: intelligent reflecting surface; cognitive radio; physical layer security; transmit beamforming; artificial noise

check for updates

Citation: Liu, Z.; Wang, J.; Jiang, H.; Wang, J.; Li, X.; Xie, W. Physical Layer Security Performance Analysis of IRS-Aided Cognitive Radio Networks. *Electronics* **2023**, *12*, 2615. https://doi.org/10.3390/electronics12122615

Academic Editor: Dimitra I. Kaklamani

Received: 19 April 2023
Revised: 6 June 2023
Accepted: 8 June 2023
Published: 9 June 2023

1. Introduction

1.1. Background

Recently, physical layer security (PLS) has been considered to guarantee that information is not eavesdropped upon. PLS has received extensive attention in wireless communication systems, and a variety of technologies for improving the security performance of wireless systems have been proposed in the existing research, such as a directional antenna design and multiple-input multiple-output (MIMO) technology. PLS is important in ensuring that information is not eavesdropped upon. Security outage probability (SOP) and average security capacity (ASC), as two important performance indicators, are the main research objects for most researchers when conducting physical layer security performance analyses. More specifically, a beamforming vector is designed at the transmitter of multiple antennas to improve PLS [1]. Another considered technology has been to transmit artificial noise (AN) from the transmitter to enhance the secrecy rate. By analyzing and optimizing the achievable secrecy capacity of the system, the authors in [2] showed that AN can improve secrecy performance by designing it to interfere with the eavesdropping channel, with an AN vector in the null space of the legitimate channel. Jointly optimizing the AN vector and beamforming vector to minimize the transmit power was proposed in [3,4], and the authors also considered the imperfect channel state information (CSI) of the eavesdropper (Eve) [4]. In addition, it has been designed for various wireless communications at present. The authors in [5] introduced an AN vector to improve the security performance of cognitive radio (CR) communication scenarios.

1.2. Prior Works

In the existing literature, the number of devices serving wireless communication has increased dramatically, and the demand for spectral efficiency has also increased. To achieve this goal, cognitive radio networks (CRNs) are extensively investigated for their capability of enhancing spectral efficiency. However, CRNs are subject to a large number of security threats, such as imitating primary user attacks, physical layer interference, and eavesdropping. Therefore, it is imperative to find a solution that balances security with other performance indicators for wireless communications. Furthermore, the intelligent reflecting surface (IRS) technology has attracted wide attention recently since it can actively adjust the phase shifts and amplitude of the channel. This indicates that the spectral and energy efficiency of wireless communication systems can be enhanced by applying IRS technology. In light of this, a variety of physical layer algorithms have been proposed for optimizing the performance of wireless communication systems. To be specific, Jiang et al. have proposed a sub-array separation algorithm for optimizing the computational complexity of the investigation of channel propagation statistics in the time domain, spatial domain, and frequency domain [6]. In [7], the authors derived the expressions of the path loss coefficients corresponding to different types of propagation links for accurately investigating channel propagation statistics. Furthermore, some researchers have developed many algorithms for validating the feasibility of using the IRS technology to assist secure wireless communication systems in different communication scenarios, such as the multiple-input single-output (MISO) case [8], UAV communication [9], millimeter wave communication [10], and CRN systems [11]. However, the application of passive IRS also brings about the “dual fading” effect, and in typical communication scenarios, passive IRS can only obtain limited channel gain. Consequently, several researchers have presented the application of active IRS in a wireless communication system for overcoming the fundamental limitations of the “dual fading” effect [12–18]. Reference [12] presented an active IRS in a single-input multiple-output system that optimizes beamforming at the receiver side and the reflection coefficient matrix of the IRS to minimize the IRS-associated noise at the receiver side and maximize the system’s received signal power. The findings showed that under the same power budget, active IRS auxiliary systems had better performance than traditional passive IRS auxiliary systems. However, both systems featured the same total power budget. If the number of reflective units in the IRS was large enough, the passive IRS brought superior channel capacity to active IRS [13]. References [14–16] also proved the advantage of active IRS over passive IRS. Notably, in contrast to the existing passive IRS that does not amplify the passive reflected signal, active IRS needs extra power for supporting the reflected signal’s active amplification. As a result, active IRS needs a larger power budget compared to passive IRS for the same reflection element number [17]. For minimizing the power loss of active IRS, a sub-connected structure of the active IRS was presented in [18] at the cost of decreasing the freedom required for the beamforming design. The components on IRS control their phase shifts independently, but they share a common power amplifier. Simulation outcomes demonstrate that the sub-connected architecture is an energy-efficient realization of active IRS. Additionally, the authors in Tsinghua University currently have mature IRS hardware design methods [19], which have prompted more researchers to investigate the favorable impact of IRS on wireless communication across various fields.

However, few of the existing works have studied IRS-aided CR systems until recently, except for a few influential papers that have been published [20,21]. The authors in [20] investigated if IRS technology could reduce the transmission power of the secondary transmitter (ST). In [21], an IRS-assisted CR system was proposed by establishing an optimization to maximize the secrecy rate of ST while a static Eve exists; cooperative beamforming was considered as well, to ensure the quality of service (QoS) of the primary receiver (PR). In addition, the IRS has been exploited to assist secure communication by cooperating with other traditional security technologies such as the AN [22], cooperative relaying [23], and power-transfer SWIPT and simultaneous wireless information [24–26]. The author in [27] employed adaptive transmit power along with energy harvesting in CRNs. Most materials supposed that the CSI was perfectly known in the receiver/transmitter. Reference [28] considered imperfect CSI in IRS-aided CRN, and analyzed safety performance. Study [29] analyzed the average block error rates (BLERs) performance for multiple IRS-aided CRN short-packet communication systems.

1.3. Motivations and Main Contributions

Due to the inclusion of PR and SR users as well as RIS devices in the CRN system, which brings more security uncertainties, it is urgent to conduct relevant research on the physical layer security of the CRN system in order to further improve its security. Inspired by CR systems and the advantages of IRS, this research considered the physical layer security of an IRS-aided CR system with AN, as presented in Figure 1. This system was equipped with a multiple-antenna secondary receiver (SR) transmitter (SR-TX), a signal antenna SR, and a primary receiver (PR). Moreover, there was a static signal antenna Eve near the SR-TX. More specifically, we introduced AN at the SR-TX to interfere with the Eve, and the problem of minimizing the transmit power of SU was considered through alternately optimizing the AN and beamforming vector as well as the phase shift matrix of IRS, while being subject to the security capacity constraint and the interference temperature constraint at the PR, and the secrecy rate constraint. In the process of solving this problem, we used iterative algorithm optimization (AO) based on the block coordinate descent (BCD) method [30] to deal with the nonconvex problem, which transformed the object problem into two subproblems, and the variables in the two subproblems were alternatively optimized. In addition, the method of semidefinite relaxation (SDR) was applied to solve the unit module constraint. A Gaussian randomization scheme from [31] was utilized to recover the rank-1 variables until the algorithm converged. The major contributions of our study are summarized as follows:

1. First, we optimize the beamforming of base stations for users, the covariance matrix of AN, as well as the phase shift matrix of IRS, which aim to ensure the basic service quality of primary users and maximize the confidentiality of secondary users.
2. Second, we propose a BCD-based alternating optimization algorithm to transform the nonconvex problem into a solvable subconvex problem, which can be used to solve nonconvex problems. Furthermore, the SDR was applied to solve the unit module constraint during the solving process.
3. Third, we use mathematically equivalent models and related approximate processing schemes to transform the physical layer security performance indicators into easily manageable convex optimization power problems, which has the advantages of greatly reducing computational complexity.

The structure of this work is concluded as follows: Section 2 presents the system model. Section 3 lists the problem formulation and proposes the optimization of the phase-shift matrix, and beamforming vector separately. Section 4 presents the numerical results, and Section 5 summarizes this study.

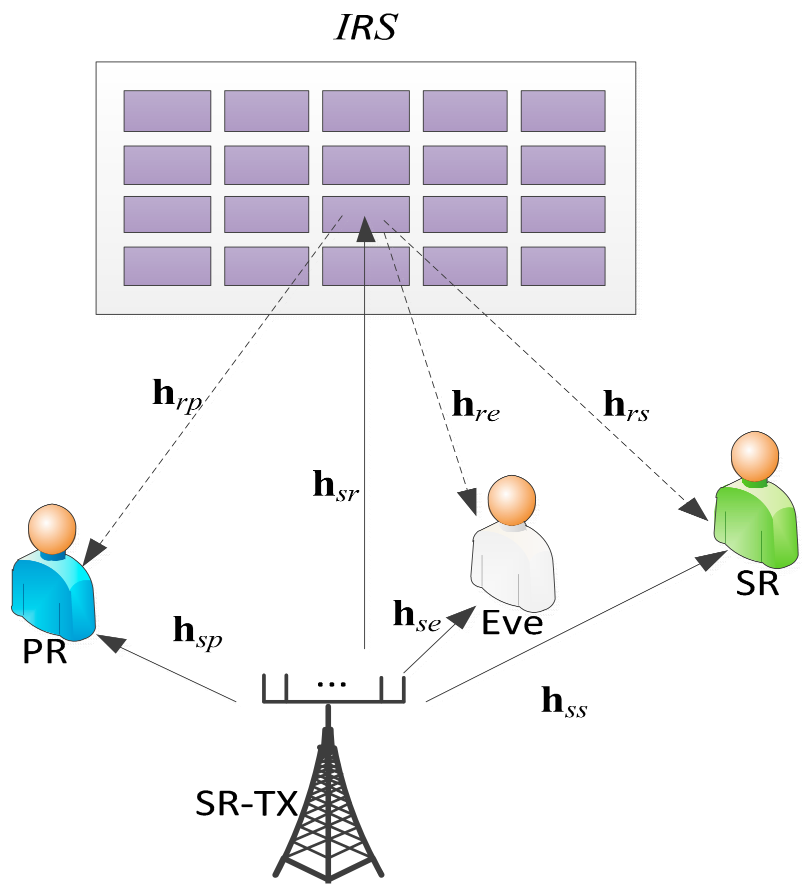

Figure 1. IRS-aided CR system with an Eve.

2. System Model

As illustrated in Figure 1, we take into account an IRS-assisted CR communication system, including a secondary receiver transmitter equipped with multiple antennas, a signal antenna SR and PR, an Eve, and an IRS that is composed of N reflecting meta-surfaces. To reduce the complexity of the system's mathematical model, this research did not consider the PR-TX. The above scenario also exists in practice, such as for user scenarios with walkie talkies that only have a reception function. Furthermore, the received signal of the PR is an interference signal whose power is constrained by the maximum interference power. Then, according to the principle of PLS, the security rate must meet the requirement that the SR capacity is larger than the Eve capacity. Under the QoS condition of meeting the PR, the electromagnetic parameters of the active IRS are optimized to maximize the security rate of the system.

2.1. Main Link

It is worth mentioning that when IRS technology is used in wireless propagation scenarios, the communication mechanism is significantly different from when we do not consider the IRS technology. In light of this, we need to adopt a novel solution to study the performance of IRS-assisted wireless communication systems. Here, we denote $\mathbf{h}_{sp} \in \mathbb{C}^{M\times 1}$ to characterize the propagation statistics of the subchannel between the SR-TX and the PR. We denote $\mathbf{h}_{ss} \in \mathbb{C}^{M\times 1}$ to characterize the propagation statistics of the subchannel between the SR-TX and the SR. We denote $\mathbf{h}_{sr} \in \mathbb{C}^{N\times M}$ to characterize the propagation statistics of the subchannel between the SR-TX and the IRS. Furthermore, the channels from the IRS to the PR and the SR are given by $\mathbf{h}_{rp} \in \mathbb{C}^{N\times 1}$ and $\mathbf{h}_{rs} \in \mathbb{C}^{N\times 1}$, respectively. The diagonal phase shift matrix of the IRS is denoted by $\boldsymbol{\phi} = diag(f_1, f_2, \cdots, f_N)$ [3], where $f_n = e^{j\theta_n}$, $n = 1, \cdots, N$, and $\theta_n \in [0, 2\pi)$ represent the phase shift of the signal transmission to each element of the IRS array.

The transmitted signal $\mathbf{x}_s$ is expressed by the following:

$$\mathbf{x}_s = \mathbf{w}s + \mathbf{z} \tag{1}$$

where $\mathbf{w} \in \mathbb{C}^{M\times 1}$ stands for the beamforming vector, and $\mathbf{z} \in \mathbb{C}^{M\times 1}$ represents the AN vector with $\mathbf{z} \sim \mathrm{CN}\,(\mathbf{Z} \geq 0)$.

The received signal reflected by the IRS at the SR can be expressed as follows:

$$y_s = \left(\mathbf{h}_{ss}^T + \mathbf{h}_{rs}^T \boldsymbol{\Phi} \mathbf{h}_{sr}\right)\mathbf{x}_s + n_s \tag{2}$$

where $n_s \sim \mathrm{CN}\left(0,\, \sigma_s^2\right)$ accounts for the complex additive white Gaussian noise (AWGN) at the SR-TX, and $\boldsymbol{\phi} \in \mathbb{C}^{N\times N}$ denotes the electromagnetic parameters of IRS. Therefore, the signal-to-interference-to-noise ratio (SINR) at SR can be given as [20]:

$$\gamma_s = \frac{\left|\widetilde{\mathbf{h}}_s \mathbf{w}\right|^2}{\left|\widetilde{\mathbf{h}}_s \mathbf{z}\right|^2 + \sigma_s^2} \tag{3}$$

where $\widetilde{\mathbf{h}}_s = \mathbf{h}_{ss}^T + \mathbf{h}_{rs}^T \boldsymbol{\phi} \mathbf{h}_{sr}$. It is worth mentioning that owing to the fact that the primary receiver transmitter (PR-TX) is not considered in our proposed model, the PR will not only receive interference from the SR, but also the signal reflected by the IRS when the SR-TX broadcasts the signal x_s. In light of this, the interference signal at the PR can be expressed as follows:

$$y_p = \left(\mathbf{h}_{sp}^T + \mathbf{h}_{rp}^T \boldsymbol{\Phi} \mathbf{h}_{sr}\right)\mathbf{x}_s + n_p, \tag{4}$$

where $n_p \sim \mathrm{CN}\left(0,\, \sigma_p^2\right)$ stands for the AWGN at the PR. Then, the interference power is given by the following:

$$I_p = \left|\widetilde{\mathbf{h}}_p \mathrm{w}\right|^2 + \left|\widetilde{\mathbf{h}}_p \mathrm{z}\right|^2, \tag{5}$$

where $\widetilde{\mathbf{h}}_p = \mathbf{h}_{sp}^T + \mathbf{h}_{rp}^T \boldsymbol{\phi} \mathbf{h}_{sr}$.

2.2. Eavesdropping Link

Let $\mathbf{h}_{se} \in \mathrm{C}^{M\times 1}$ denote the channels from the SR-TX to the Eve, while the transmitted signal from the IRS to the Eve is denoted by $\mathbf{h}_{se} \in \mathrm{C}^{N\times 1}$. The received signal reflected by the IRS at the Eve can be expressed as follows [32,33]:

$$y_e = \left(\mathbf{h}_{se}^T + \mathbf{h}_{re}^T \boldsymbol{\Phi} \mathbf{h}_{sr}\right)\mathbf{x}_s + n_e, \tag{6}$$

where $n_e \sim \mathrm{CN}\left(0,\, \sigma_\mathrm{e}^2\right)$ stands for the AWGN at the Eve. In the following part, the expression of the SINR at the Eve can be written as follows:

$$\gamma_e = \frac{\left|\widetilde{\mathbf{h}}_e \mathbf{w}\right|^2}{\left|\widetilde{\mathbf{h}}_e \mathbf{z}\right|^2 + \sigma_e^2}, \tag{7}$$

where $\widetilde{\mathbf{h}}_s = \mathbf{h}_{se}^T + \mathbf{h}_{re}^T \boldsymbol{\phi} \mathbf{h}_{sr}$.

3. Problem Formulation

In this section, we jointly optimize the AN vector $\mathbf{z}$ and beamforming vector $\mathbf{w}$, as well as the reflecting phase θ of the IRS to minimize the transmit power at SR-TX. In other cases, the constraints are summarized in the following parts.

3.1. Interference Power Constraint

Let ϕ_p denote the upper bound of interference power at the PR. According to existing research on passive IRS technology, passive IRS cannot amplify incident signals. Therefore, the noise generated by the amplified signal in the active IRS is ignored during the reflection process. Then, the constraint of interference power (IP) can be expressed as follows:

$$\left|\widetilde{\mathbf{h}}_p\mathbf{w}\right|^2 + \left|\widetilde{\mathbf{h}}_p\mathbf{z}\right|^2 < \phi_p. \tag{8}$$

3.2. Secrecy Rate Constraints

In the secure communication scenario shown in Figure 1, consider the case where the IRS is a passive IRS. Since passive IRS regulates only the phase of the incident signal, the amplification factor is set to 1. The system's safety rate can be given as below:

$$R_s(\mathbf{\Phi}) = \log\left(\frac{1+\gamma_s}{1+\gamma_e}\right).$$

To make sure that the SR can properly decode the transmit signal s from SR-TX, we transform the SR's achievable rate into the following SINR constraint:

$$\frac{\left|\widetilde{\mathbf{h}}_s\mathbf{w}\right|^2}{\left|\widetilde{\mathbf{h}}_s\mathbf{z}\right|^2 + \sigma_s^2} \geq \overline{\gamma}_s \tag{9}$$

where $\overline{\gamma}_s$ represents the minimum required SINR at the SR.

Similarly, the Eve cannot eavesdrop useful information; thus, the Eve's SINR constraint can be given by the following:

$$\frac{\left|\widetilde{\mathbf{h}}_e\mathbf{w}\right|^2}{\left|\widetilde{\mathbf{h}}_e\mathbf{z}\right|^2 + \sigma_e^2} \leq \overline{\gamma}_e \tag{10}$$

where $\overline{\gamma}_e$ denotes the upper bound of the SINR of the eavesdropping link to obtain the information from SR-TX.

3.3. Phase Constraint

An IRS has the advantage of adjusting the phase and amplitude of the channel [3]. However, in this research, we assumed that the IRS reflects the signal without changing the amplitude of the signals. Thus, the constraint can be written as follows:

$$|f_i| = 1, \quad i = 1, 2, \ldots, N \tag{11}$$

Based on the above constraints, the problem of maximizing the safety rate can be expressed as $\max_{\mathbf{\Phi}} R_s(\mathbf{\Phi})$, which is a nonconvex optimization problem that is difficult to handle in its current form. Since IPC is nonconvex, it is difficult to convert the unit modulus constraint (11) into a convex constraint condition when optimizing phase shift $\mathbf{\Phi}$. In addition, the objective function is also a fractional form. Therefore, the above nonconvex optimization can be translated into the problem of transmitting power miniaturization using the Dinkelbach method, which can be expressed as follows:

$$\text{(P0):} \min_{\mathbf{z},\mathbf{w},\boldsymbol{\theta}} \; Tr(\mathbf{W}+\mathbf{Z}) \tag{12}$$

$$\text{s.t. } (8), (9), (10), (11) \tag{13}$$

$$\mathbf{Z} \succeq 0 \tag{14}$$

$$\mathbf{W}\succeq 0 \tag{15}$$

$$\mathrm{rank}(\mathbf{W}) = 1 \tag{16}$$

where $\mathbf{W} = \mathbf{w}\mathbf{w}^H$ satisfies (15) and (16), while $\mathbf{Z} = \mathbf{z}\mathbf{z}^H$ satisfies (14). To the best of our knowledge, it is difficult to solve P0. First, the constraint of the unit modulus in (11) is not easy to convert into a tractable convex form when we optimize θ. Second, the objective function (OF) is in a semi-closed form. Lastly, both the OF (11) and constraints (8) contain coupled optimization variables.

4. Proposed Solutions

In this section, the proposed method is mainly divided into two steps to solve the P0. First, the beamforming vector $\mathbf{w}$ and AN vector $\mathbf{z}$ at the SR-TX are jointly optimized when phase shift f_i of the IRS is given. Then, with fixed $\mathbf{w}$ and $\mathbf{z}$, f_i is optimized to minimize the transmit power. Specifically, two subproblems, P0-A and P0-B of P0, can be written as follows:

(1) P0-A: $\min\limits_{\mathbf{z},\mathbf{w}} \mathrm{Tr}(\mathbf{W}+\mathbf{Z})$ s.t. (8), (9), (10), (14), (15), (16)

(2) P0-B: $\min\limits_{\theta} \mathrm{Tr}(\mathbf{W}+\mathbf{Z})$ s.t. (8), (9), (10), (11).

Then, we continuously update the values of f_i, $\mathbf{w}$, and $\mathbf{z}$ through the AO of these two subproblems until the OF $\mathrm{Tr}(\mathbf{W}+\mathbf{Z})$ converges.

4.1. Optimization of *W* and *Z*

Dealing with the constraints (12), we denote the following:

$$\begin{aligned} \mathbf{h}_{rs}^T\mathbf{\Phi}\mathbf{h}_{sr} &= \mathbf{f}^T diag\left(\mathbf{h}_{rs}^T\right)\mathbf{h}_{\mathrm{sr}} = \mathbf{f}^T\mathbf{G}_s \\ \mathbf{h}_{rp}^T\mathbf{\Phi}\mathbf{h}_{sr} &= \mathbf{f}^T diag\left(\mathbf{h}_{rp}^T\right)\mathbf{h}_{\mathrm{sr}} = \mathbf{f}^T\mathbf{G}_p \\ \mathbf{h}_{re}^T\mathbf{\Phi}\mathbf{h}_{sr} &= \mathbf{f}^T diag\left(\mathbf{h}_{re}^T\right)\mathbf{h}_{\mathrm{sr}} = \mathbf{f}^T\mathbf{G}_e \end{aligned} \tag{17}$$

where $\mathbf{f}\ [f_1,\cdots,f_N]^T$, $f_n\ \mathrm{e}^{j\theta_n}$, $\forall n \in 1,\cdots,N$. Then, we denote $\widetilde{\mathbf{G}}_s = \left[\mathbf{G}_s;\mathbf{h}_{ss}^T\right]$, $\widetilde{\mathbf{G}}_p = \left[\mathbf{G}_p;\mathbf{h}_{sp}^T\right]$, $\widetilde{\mathbf{G}}_e = \left[\mathbf{G}_e;\mathbf{h}_{se}^T\right]$ and $\widetilde{\mathbf{f}} = [\mathbf{f};1]$; letting $\widetilde{\mathbf{F}} = \widetilde{\mathbf{f}}\widetilde{\mathbf{f}}^H$ satisfy $\widetilde{\mathbf{F}} \geq 0$ and $\mathrm{rank}\left(\widetilde{\mathbf{F}}\right) = 1$, we have the following:

$$\begin{aligned} \widetilde{\mathbf{h}}_s &= \mathbf{h}_{ss} + \mathbf{h}_{rs}^T\mathbf{\Phi}\mathbf{h}_{sr} = \widetilde{\mathbf{f}}^T\widetilde{\mathbf{G}}_s \\ \widetilde{\mathbf{h}}_p &= \mathbf{h}_{sp} + \mathbf{h}_{rp}^T\mathbf{\Phi}\mathbf{h}_{sr} = \widetilde{\mathbf{f}}^T\widetilde{\mathbf{G}}_p \\ \widetilde{\mathbf{h}}_e &= \mathbf{h}_{se} + \mathbf{h}_{re}^T\mathbf{\Phi}\mathbf{h}_{sr} = \widetilde{\mathbf{f}}^T\widetilde{\mathbf{G}}_e. \end{aligned} \tag{18}$$

Then, P0 has the same optimal solutions as the following:

$$(\mathrm{P1}): \min_{\mathbf{Z},\mathbf{W},\widetilde{\mathbf{F}}} \mathrm{Tr}(\mathbf{W}) + \mathrm{Tr}(\mathbf{Z}) \tag{19}$$

$$s.t.\mathbf{Z},\mathbf{W},\widetilde{\mathbf{F}} \succeq 0, \mathrm{rank}\left(\widetilde{\mathbf{F}}\right) = 1 \tag{20}$$

$$\frac{\mathrm{Tr}\left(\widetilde{\mathbf{F}}\widetilde{\mathbf{G}}_s\mathbf{W}\widetilde{\mathbf{G}}_s^H\right)}{\mathrm{Tr}\left(\widetilde{\mathbf{F}}\widetilde{\mathbf{G}}_s\mathbf{Z}\widetilde{\mathbf{G}}_s^H\right) + \sigma_s^2} > \overline{\gamma}_s \tag{21}$$

$$\frac{\mathrm{Tr}\left(\widetilde{\mathbf{F}}\widetilde{\mathbf{G}}_e\mathbf{W}\widetilde{\mathbf{G}}_e^H\right)}{\mathrm{Tr}\left(\widetilde{\mathbf{F}}\widetilde{\mathbf{G}}_e\mathbf{Z}\widetilde{\mathbf{G}}_e^H\right) + \sigma_e^2} < \overline{\gamma}_e \tag{22}$$

$$\mathrm{Tr}\left(\widetilde{\mathbf{F}}\widetilde{\mathbf{G}}_p\mathbf{W}\widetilde{\mathbf{G}}_p^H\right)+\mathrm{Tr}\left(\widetilde{\mathbf{F}}\widetilde{\mathbf{G}}_p\mathbf{Z}\widetilde{\mathbf{G}}_p^H\right)<\phi_p. \tag{23}$$

Both problem P1 and all of the constraints become convex after processing. Fixing either $\{\mathbf{Z},\mathbf{W}\}$ or $\widetilde{\mathbf{F}}$, the subproblem becomes solvable. When an initial value of $\widetilde{\mathbf{F}}$ is given, problem P1 can be rewritten as problem P1a:

$$(\mathrm{P}1a):\quad \min_{\mathbf{Z},\mathbf{w}}\quad \mathrm{Tr}(\mathbf{W})+\mathrm{Tr}(\mathbf{Z}) \tag{24}$$

$$s.t.\quad \mathbf{Z},\mathbf{W}\succeq 0 \tag{25}$$

$$\frac{\mathrm{Tr}(\mathbf{\Psi}_s\mathbf{W})}{\mathrm{Tr}(\mathbf{\Psi}_s\mathbf{Z})+\sigma_s^2}>\overline{\gamma}_s \tag{26}$$

$$\frac{\mathrm{Tr}(\mathbf{\Psi}_e\mathbf{W})}{\mathrm{Tr}(\mathbf{\Psi}_e\mathbf{Z})+\sigma_e^2}<\overline{\gamma}_e \tag{27}$$

$$\mathrm{Tr}\left(\mathbf{\Psi}_p\mathbf{W}\right)+\mathrm{Tr}\left(\mathbf{\Psi}_p\mathbf{Z}\right)<\phi_p \tag{28}$$

where $\boldsymbol{\psi}_s=\widetilde{\mathbf{G}}_s^H\widetilde{\mathbf{F}}\widetilde{\mathbf{G}}_s$, $\boldsymbol{\psi}_p=\widetilde{\mathbf{G}}_p^H\widetilde{\mathbf{F}}\widetilde{\mathbf{G}}_p$, and $\boldsymbol{\psi}_e=\widetilde{\mathbf{G}}_e^H\widetilde{\mathbf{F}}\widetilde{\mathbf{G}}_e$. Thus, we can use CVX tools to find the optimal solution of P1a [34]. However, in principle, if the rank of the obtained $\mathbf{W}$ matrix is not equal to 1, the Gaussian randomization method can be used to convert the rank to 1, and then the matrix $\mathbf{W}$ can be obtained by using the eigenvalue decomposition.

4.2. Optimization of Phase Matrix $\widetilde{\mathrm{F}}$

In the second step, we fix the variable $\{\mathbf{W},\mathbf{Z}\}$; the subproblem of P0b is easier to handle. We first reformulate the constraint in (9) and (10). Specifically, it can be simplified as follows:

$$\begin{aligned}
&\frac{\widetilde{\mathbf{h}}_s^H\mathbf{W}\widetilde{\mathbf{h}}_s}{\widetilde{\mathbf{h}}_s^H\mathbf{Z}\widetilde{\mathbf{h}}_s+\sigma_s^2}\geq\overline{\gamma}_s\\
&\Leftrightarrow \mathrm{Tr}\left([\mathbf{W}-\overline{\gamma}_s\mathbf{Z}]\widetilde{\mathbf{h}}_s\widetilde{\mathbf{h}}_s^H\right)\geq\overline{\gamma}_s\sigma_s^2\\
&\Leftrightarrow \mathrm{Tr}\left([\mathbf{W}-\overline{\gamma}_s\mathbf{Z}]\left(\widetilde{\mathbf{G}}_s^H\widetilde{\mathbf{f}}\right)\left(\widetilde{\mathbf{f}}^H\widetilde{\mathbf{G}}_s\right)\right)\geq\overline{\gamma}_s\sigma_s^2\\
&\Leftrightarrow \mathrm{Tr}\left(\widetilde{\mathbf{G}}_s[\mathbf{W}-\overline{\gamma}_s\mathbf{Z}]\widetilde{\mathbf{G}}_s^H\widetilde{\mathbf{F}}\right)\geq\overline{\gamma}_s\sigma_s^2
\end{aligned} \tag{29}$$

$$\begin{aligned}
&\frac{\widetilde{\mathbf{h}}_e^H\mathbf{W}\widetilde{\mathbf{h}}_e}{\widetilde{\mathbf{h}}_e^H\mathbf{Z}\widetilde{\mathbf{h}}_e+\sigma_e^2}\leq\overline{\gamma}_e\\
&\Leftrightarrow \mathrm{Tr}\left([\mathbf{W}-\overline{\gamma}_e\mathbf{Z}]\widetilde{\mathbf{h}}_e\widetilde{\mathbf{h}}_e^H\right)\leq\overline{\gamma}_e\sigma_e^2\\
&\Leftrightarrow \mathrm{Tr}\left([\mathbf{W}-\overline{\gamma}_e\mathbf{Z}]\left(\widetilde{\mathbf{G}}_e^H\widetilde{\mathbf{f}}\right)\left(\widetilde{\mathbf{f}}^H\widetilde{G}_e\right)\right)\leq\overline{\gamma}_e\sigma_e^2\\
&\Leftrightarrow \mathrm{Tr}\left(\widetilde{\mathbf{G}}_e[\mathbf{W}-\overline{\gamma}_e\mathbf{Z}]\widetilde{\mathbf{G}}_e^H\widetilde{\mathbf{F}}\right)\leq\overline{\gamma}_e\sigma_e^2
\end{aligned} \tag{30}$$

Then, slack variables are introduced into the SINR constraint of the SR in (29) and Eve in (30), which can be rewritten as the following, respectively:

$$\mathrm{Tr}\left(\widetilde{\mathbf{G}}_s[\mathbf{W}-\overline{\gamma}_s\mathbf{Z}]\widetilde{\mathbf{G}}_s^H\widetilde{\mathbf{F}}\right)\geq\overline{\gamma}_s\sigma_s^2+\delta_0,\delta_0\geq 0 \tag{31}$$

$$\mathrm{Tr}\left(\widetilde{\mathbf{G}}_e[\mathbf{W}-\overline{\gamma}_e\mathbf{Z}]\widetilde{\mathbf{G}}_e^H\widetilde{\mathbf{F}}\right)\leq\overline{\gamma}_e\sigma_e^2-\delta_1,\delta_1\geq 0. \tag{32}$$

Finally, P0b is rewritten as follows:

$$(\mathrm{P}2):\ \max_{\widetilde{f},\delta}\quad \|\delta\|_1 \tag{33}$$

$$\text{s.t.} \quad \mathrm{Tr}\left(\widetilde{\mathbf{G}}_s[\mathbf{W}-\overline{\gamma}_s\mathbf{Z}]\widetilde{\mathbf{G}}_s^H\widetilde{\mathbf{F}}\right) \geq \overline{\gamma}_s\sigma_s^2+\delta_0 \tag{34}$$

$$\mathrm{Tr}\left(\widetilde{\mathbf{G}}_e[\mathbf{W}-\overline{\gamma}_e\mathbf{Z}]\widetilde{\mathbf{G}}_e^H\widetilde{\mathbf{F}}\right)+\delta_1 \leq \overline{\gamma}_e\sigma_e^2 \tag{35}$$

$$\mathrm{Tr}\left(\mathbf{\Lambda}_p\widetilde{\mathbf{F}}\right)+\mathrm{Tr}\left(\mathbf{V}_p\widetilde{\mathbf{F}}\right) < \phi_p \tag{36}$$

$$\delta \succeq 0 \tag{37}$$

$$\left|\widetilde{\mathbf{f}}_n\right| = 1, n=1,\cdots,N \tag{38}$$

where $\delta=[\delta_0,\delta_1]^H$, $\mathbf{\Lambda}_P=\widetilde{\mathbf{G}}_P\mathbf{W}\widetilde{\mathbf{G}}_p^H$, and $\mathbf{V}_P=\widetilde{\mathbf{G}}_P\mathbf{Z}\widetilde{\mathbf{G}}_p^H$. Therefore, we observe that the constraint of (38) in P3 is the unit modulus constraint. According to [22], we can use a semidefinite programming (SDP) method to handle the constraint. Thus, P2 can be rewritten as follows:

$$(\mathrm{P2}a):\ \max_{\mathbf{F},\delta}\quad \|\delta\|_1 \tag{39}$$

$$\text{s.t.} \quad (34),(35),(36),(37) \tag{40}$$

$$diag\left(\widetilde{\mathbf{F}}\right)=1_N \tag{41}$$

$$\widetilde{\mathbf{F}} \succeq 0 \tag{42}$$

$$\mathrm{rank}\left(\widetilde{\mathbf{F}}\right)=1 \tag{43}$$

where constraints (41)–(43) replace constraint (38). To the best of our knowledge, all of the constraints of P2a are convex except for (43). Therefore, we can use the semidefinite relaxation (SDR) method to handle constraint (43), but it is not guaranteed that all of the $\widetilde{\mathbf{F}}$ matrices we obtain have rank 1, so that $\widetilde{\mathbf{f}}_n$ cannot be solved using eigenvalue decomposition. To avoid these types of situations, the most effective method is to use Lemma 1, which can be summarized as follows:

Lemma 1. *Any positive semidefinite matrix* $\mathbf{A}$ *satisfies the inequality [4]:*

$$|\mathbf{I}+\mathbf{A}| \geq 1+\mathrm{Tr}(\mathbf{A}) \tag{44}$$

and the equality in (44) holds if, and only if $\mathrm{rank}(\mathbf{A}) \leq 1$. *Then, constraint (43) can be recast as follows:*

$$\begin{aligned}(43)\quad &\Leftrightarrow \left|\mathrm{I}+\widetilde{\mathbf{F}}\right| \geq 1+\mathrm{Tr}\left(\widetilde{\mathbf{F}}\right)\\ &\Leftrightarrow \log\det\left|\mathrm{I}+\widetilde{\mathbf{F}}\right| \geq \log(1+(N+1))\end{aligned} \tag{45}$$

where $\mathrm{Tr}\left(\widetilde{\mathbf{F}}\right)=N+1$. *Using the penalty-based method, P2a is rewritten as follows:*

$$(\mathrm{P2b}):\ \max_{\mathbf{F},\delta}\quad \|\delta\|_1+\kappa\left[\log(1+(N+1))-\log\det\left(\mathrm{I}+\widetilde{\mathbf{F}}\right)\right] \tag{46}$$

$$\text{s.t.} \quad (40),(41),(42) \tag{47}$$

where κ denotes a penalty factor whose aim is to penalize the case of $\mathrm{rank}\left(\widetilde{\mathbf{F}}\right) \neq 1$*. However, it is difficult to solve, because* $\log\det\left(\mathrm{I} + \widetilde{\mathbf{F}}\right)$ *is a concave function about* $\widetilde{\mathbf{F}}$*. Utilizing a first-order Taylor series, we obtain the upper bound approximately as follows:*

$$\log\det\left(\mathrm{I} + \widetilde{\mathbf{F}}\right) \leq (\log e) Tr\left\{ \left(\left(\mathrm{I} + \widetilde{\mathbf{F}}^{(n)}\right)^{-1} \right)^{*} \left(\widetilde{\mathbf{F}} - \widetilde{\mathbf{F}}^{(n)}\right) \right\} + (\log e) \log\det\left(\mathrm{I} + \widetilde{\mathbf{F}}^{(n)}\right) \tag{48}$$

where e is the natural logarithm. Finally, P2b is recast as the following:

$$(\mathrm{P2}c): \max_{\mathrm{F},\delta} \|\delta\|_1 + \kappa\left[-(\log e) Tr\left\{ \left(\left(\mathrm{I} + \mathrm{F}^{(n)}\right)^{-1} \right)^{*} \left(\mathrm{F} - F^{(n)}\right) \right\} \right] \tag{49}$$

$$\text{s.t.} \quad (40), (41), (42). \tag{50}$$

After processing the above, P2c can be solved using CVX tools. The whole AO algorithm is shown in Algorithm 1. Convergence of transmitting power can be ensured through the iterative optimization of P1a and P2c.

Algorithm 1 Alternating Optimization Algorithm

Input: N, M, h.
Output: $\widetilde{\mathbf{F}}^{*}$, $\mathbf{W}^{*}$, $\mathbf{Z}^{*}$.
Initialize $\widetilde{\mathbf{F}}_0$ by random generation.
repeat
  Obtain $\mathbf{W}_i$ and $\mathbf{Z}_i$ by solving (P1a) in (24) for given $\widetilde{\mathbf{F}}_i$.
    if $\mathrm{rank}(\mathbf{W}) \neq 1$ or $\mathrm{rank}(\mathbf{Z}) \neq 1$
      Gaussian randomization algorithm;
    end
  Obtain $\widetilde{\mathbf{F}}_{i+1}$ by solving (P2c) in (49) for given $\mathbf{W}_i$ and $\mathbf{Z}_i$.
    if $\mathrm{rank}\left(\widetilde{\mathbf{F}}_{i+1}\right) \neq 1$
      Gaussian randomization algorithm;
    end
  compute $P_{i+1} = \mathrm{Tr}(\mathbf{W}_i) + \mathrm{Tr}(\mathbf{Z}_i)$.
  Update $i \leftarrow i + 1$
until $P_{i+1} - P_i \leq 1e - 3$.

5. Numerical Results

We assumed that the SR-TX, the SR, the PR, the Eve, and the IRS were located at (0, 10), (180, 0), (160, 0), (170, 0), and (100, 25) in meters (m) on a two-dimensional plane [3], respectively. The channels of the SR-TX-Eve, SR-TX-SR, and SR-TX-PR experienced Rayleigh fading, while the IRS-SR, SR-TX-IRS, IRS-Eve, and IRS-PR links all experienced Rician fading with a Rician factor of 4. The path loss index from ST to all user links was set to 3, the path loss index from ST to IRS links was set to 2.5, and the path loss index from the IRS to all user links was set to 2.5. The 'passive IRS' in the simulation diagram denotes the simulation curve when IRS is present, while the others represent the simulation curve of the active IRS-assisted CR system under the corresponding parameter settings. The large-scale fading was defined as $10^{-3}d^{-c}$, in which d and c stand for the link distance and path loss exponent, respectively. The other default system parameters were set as follows: $\sigma_s^2 = \sigma_e^2 = \sigma_p^2 = -65$ dBm, $\overline{\gamma}_s = 8$, $\overline{\gamma}_e = 2$, and $\phi_p = -35$ dBm.

In Figure 2, the relationship curve between different transmission powers and the average security rate of ST is shown. The number of reflection units for IRS was set to $N = 16$. Among them, "passive IRS" denotes the simulation curve when the IRS is present, and "$P_A = 20$ dBm" stands for the simulation curve of the safety rate that can be reached with a 20 dBm maximal noise amplification power for active IRS. Under identical parameter settings, the safety properties of passive IRS together with the active IRS-assisted CR systems were compared. The maximum interference power received by the PR was $P_I = 10$ dBm. As P_t increased, the average security rate of the SR end also continued to increase and showed a trend of convergence. In the case of active IRS, the maximum amplification amplitude coefficient of each reflection unit was set to $\alpha^2_{\max} = 30$ dB. Two cases of the maximum noise amplification power of an active IRS were considered: $P_A = 30$ dBm and $P_A = 20$ dBm. From the figure, it can be seen that when the transmission power was the same, active IRS always provided a superior safety performance gain relative to passive IRS. This is attributed to the fact that active IRS can tune the phase of the incident signal and simultaneously amplify the incident signal, and the channel capacity at the SR end thus increased further. However, active IRS amplifies the incoming signal while also amplifying the introduced thermal noise. The simulation outcomes show that the average safety rate of different amplified noise power budgets is basically the same when the transmission power is small. This indicates that under low transmission power conditions, the noise power budget of the active IRS had little effect on the system's safety performance. When the transmission power was high, the average safe rate increased with increasing P_A. Then, as the transmission power increased to a certain value, the safety rate curve gradually smoothed out; even at $P_t = 40$ dBm, the average safe rate of the "$P_A = 20$ dBm" and "passive IRS" curves were almost the same. This is because when the threshold value of amplified noise power is low and the transmission power is high, the amplification of the incident signal by the active IRS will also be limited according to the constraints of amplified noise. In addition, in the case of "passive IRS", due to the limitation of the PR end interference power threshold condition $P_I = 10$ dBm, when power was raised to a certain value, the channel gain brought by the reflection link continued to weaken until $P_I = 10$ dBm, and the average safety rate no longer increased. Based on the aforementioned observations, we can conclude that the security rate is lower in scenarios without RIS or AN compared to systems with RIS and AN, and RIS brings higher security rates than AN. These results are in agreements with the ones in [14,15], which further demonstrates the accuracy of the aforementioned conclusions.

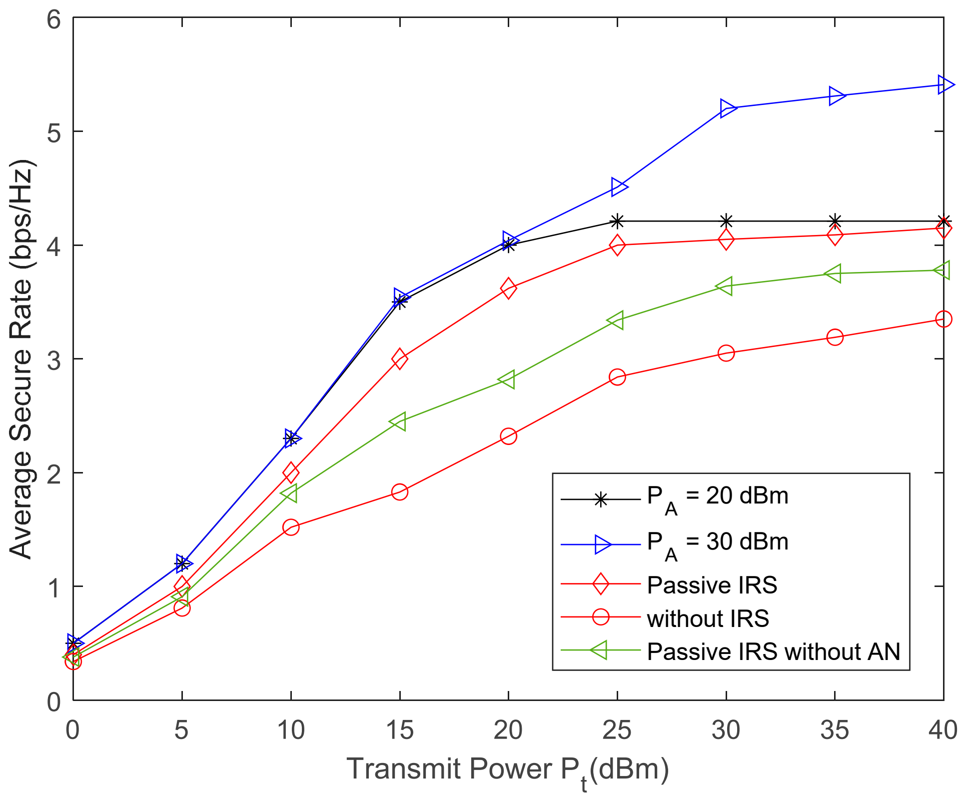

Figure 2. Average security rates with different transmission powers P_t when $N = 16$.

In Figure 3, the average security rate curves of the active IRS- and passive IRS-assisted CR systems with different amplitudes were compared under different transmission powers of ST. Setting $N = 32$, $P_A = 30$ dBm, and $P_I = 10$ dBm, the average safety rates under different $\alpha^2_{\max}$ conditions were compared. As shown in Figure 3, the average safety rate increased as $\alpha^2_{\max}$ increased. Especially when the reflection power was less than 15 dBm, the safe rate curves of different amplification amplitudes were basically consistent. Under weak power conditions, the security rate was not sensitive to the amplification gain of the active IRS. When the transmission power was greater than 15 dBm, as the amplification amplitude increased, the average security rate also increased. Active IRS achieved better safety performance in contrast to passive IRS. Furthermore, as the PA value increased, the average safety rate also increased, especially when P_t was greater than 15 dBm.

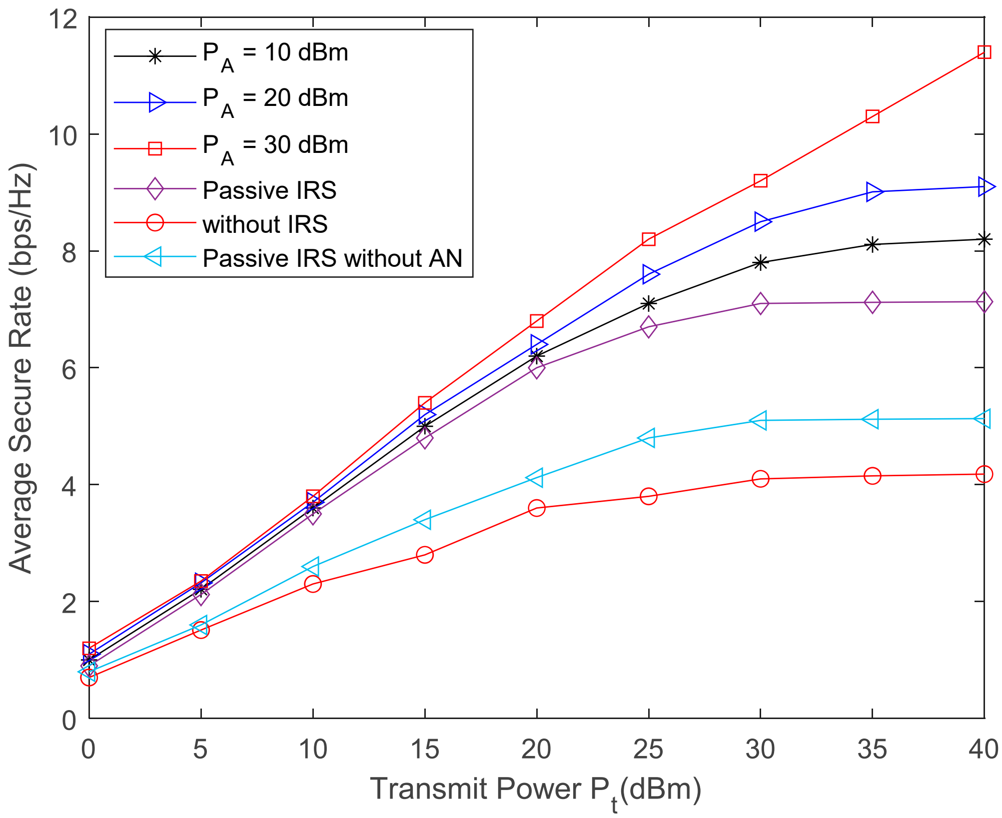

Figure 3. Average security rates with different transmission powers P_t when $N = 32$.

Figure 4 shows the transmitted power curves for different numbers of reflection units. It is obvious that when $N > 3$, the transmitted power decreased with an increase in the number of reflection units, which is consistent with the results in [6], thereby demonstrating the accuracy of the aforementioned conclusions. It is thus shown that the IRS can guarantee the security of CR systems with low power consumption. Furthermore, it can be seen that the convergence times of the algorithm gradually increased with an increase in the value of N. This can be explained by the fact that when we increase the number of elements in the IRS array, which results in the dimension of the phase matrix $\mathbf{\Phi}$ having larger values, more computation time and iterations are required to optimize the value of $\mathbf{\Phi}$. It can be concluded that when the communication systems are equipped with more elements of the IRS array, they can reduce the transmit power of the SR-TX. However, they will increase the time complexity of the algorithm.

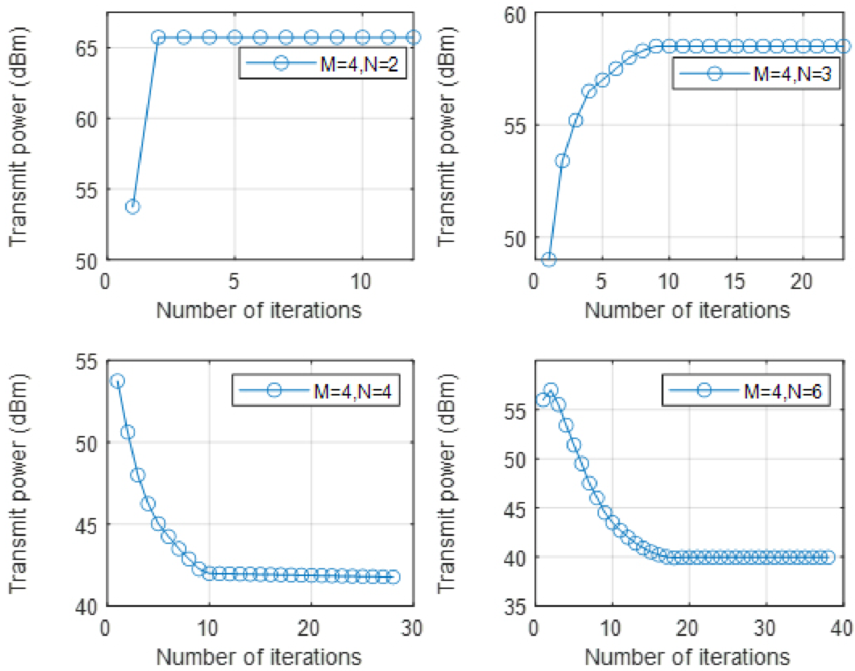

Figure 4. Convergence of the presented algorithm for various values of *N*.

Figure 5 shows the transmitted power curves for different numbers of antennas. We can observe that the number of iterations decreased when the proposed algorithm converged with the increase in the number of antennas. Moreover, less transmit power was required as the number of antennas of the SR-TX decreased when fixing the IRS elements. Based on the aforementioned observations, we can conclude that the number of IRS elements and transmit antennas can be increased appropriately if the transmit power of the SR-TX is limited, while meeting the constraints of secure communication, which is in agreement with the conclusions in [23,24], thereby demonstrating the correctness of the above simulated results.

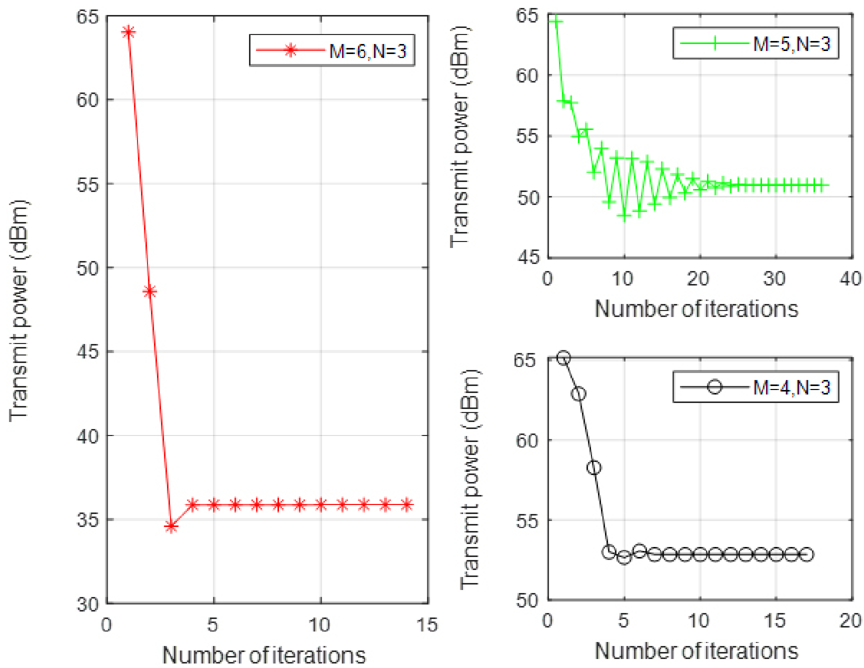

Figure 5. Convergence of the presented algorithm for various values of *M*.

6. Conclusions

In this article, we have investigated a system's secrecy performance by introducing an AN vector at the SR-TX to design an IRS-aided wireless communication system. The OF minimized the transmit power of the SR-TX by alternating optimization of the beamforming vector and the AN, and phase shift matrix of the IRS while being subject to an IT and secrecy rate constraint of PR. To solve the challenge constraint, the AO algorithm was utilized. Utilizing the SDR scheme, we dealt with the $\{\mathbf{W}, \mathbf{Z}\}$ and θ_i effectively. For the constraint of the unit modulus, the penalty function method was applied. Simulation results illustrate that the joint scheme effectively reduced the transmit power at the SR-TX under the condition of ensuring secure communication. At the same time, the QoS of the PR was satisfied.

As for future research directions, we can carry out measurements to further confirm the simulated results of the presented algorithm. Furthermore, we can further optimize the proposed algorithm to enhance the properties of the IRS-aided wireless communication system. In addition, we can further optimize the proposed algorithm based on the assumption that the CSI was not perfect in the IRS-aided cognitive radio network.

Author Contributions: Formal analysis, J.W. (Jun Wang); Investigation, J.W. (Ji Wang); Writing—original draft, Z.L.; Visualization, X.L.; Supervision, W.X.; Funding acquisition, H.J. All authors have read and agreed to the published version of the manuscript.

Funding: This work was supported in part by the National Natural Science Foundation of China under Grant 62101205, in part by the Natural Science Foundation of Hunan Province under Grant 2023JJ50045 and 2023JJ50046, in part by the Key Research and Development Program of Hubei Province under Grant 2021BAA170, in part by the Natural Science Foundation of Hubei Province under Grant 2021CFB248, and in part by the Open Fund of Advanced Cryptography and System Security Key Laboratory of Sichuan Province under Grant SKLACSS-202115.

Data Availability Statement: Available online: https://sice.hnist.cn/info/1289/7182.htm (accessed on 5 June 2023).

Conflicts of Interest: The authors declare no conflict of interest.

References

1. Trindade, S.; da Fonseca, N.L. Channel modeling and characteristics analysis for 6G wireless communications. *IEEE Netw.* **2021**, *35*, 296–303.
2. Hong, S.; Pan, C.; Ren, H.; Wang, K.; Nallanathan, A. Artificial-Noise-Aided Secure MIMO Wireless Communications via Intelligent Reflecting Surface. *IEEE Trans. Commun.* **2020**, *68*, 7851–7866. [CrossRef]
3. Wu, Q.; Zhang, R. Towards Smart and Reconfigurable Environment: Intelligent Reflecting Surface Aided Wireless Network. *IEEE Commun. Mag.* **2020**, *58*, 106–112. [CrossRef]
4. Hong, S.; Pan, C.; Ren, H.; Wang, K.; Chai, K.K.; Nallanathan, A. Robust Transmission Design for Intelligent Reflecting Surface-Aided Secure Communication Systems with Imperfect Cascaded CSI. *IEEE Trans. Wirel. Commun.* **2020**, *20*, 2487–2501. [CrossRef]
5. Nguyen, V.-D.; Duong, T.Q.; Dobre, O.A.; Shin, O.-S. Joint Information and Jamming Beamforming for Secrecy Rate Maximization in Cognitive Radio Networks. *IEEE Trans. Inf. Forensics Secur.* **2016**, *11*, 2609–2623. [CrossRef]
6. Jiang, H.; Xiong, B.; Zhang, H.; Basar, E. Physics-Based 3D End-to-End Modeling for Double-RIS Assisted Non-stationary UAV-to-Ground Communication Channels. *IEEE Trans. Commun.* **2023**. [CrossRef]
7. Jiang, H.; Xiong, B.; Zhang, H.; Basar, E. Hybrid Far- and Near-field Modeling for Reconfigurable Intelligent Surface Assisted V2V Channels: A Sub-Array Partition Based Approach. *IEEE Trans. Wirel. Commun.* **2023**. [CrossRef]
8. Yu, X.; Xu, D.; Schober, R. Enabling Secure Wireless Communications via Intelligent Reflecting Surfaces. In Proceedings of the 2019 IEEE Global Communications Conference (GLOBECOM) 2019, Waikoloa, HI, USA, 9–13 December 2019; pp. 1–6. [CrossRef]
9. Fang, S.; Chen, G.; Li, Y. Joint Optimization for Secure Intelligent Reflecting Surface Assisted UAV Networks. *IEEE Wirel. Commun. Lett.* **2020**, *10*, 276–280. [CrossRef]
10. Lu, X.; Yang, W.; Guan, X.; Wu, Q.; Cai, Y. Robust and Secure Beamforming for Intelligent Reflecting Surface Aided mmWave MISO Systems. *IEEE Wirel. Commun. Lett.* **2020**, *9*, 2068–2072. [CrossRef]
11. Guan, X.; Wu, Q.; Zhang, R. Joint Power Control and Passive Beamforming in IRS-Assisted Spectrum Sharing. *IEEE Commun. Lett.* **2020**, *24*, 1553–1557. [CrossRef]
12. Long, R.; Liang, Y.-C.; Pei, Y.; Larsson, E.G. Active Reconfigurable Intelligent Surface-Aided Wireless Communications. *IEEE Trans. Wirel. Commun.* **2021**, *20*, 4962–4975. [CrossRef]

13. Zhi, K.; Pan, C.; Ren, H.; Chai, K.K.; Elkashlan, M. Active IRS versus passive IRS: Which is superior with the same power budget? *arXiv* **2021**, arXiv:2112.07510.
14. Khoshafa, M.H.; Ngatched, T.M.N.; Ahmed, M.H.; Ndjiongue, A.R. Active Reconfigurable Intelligent Surfaces-Aided Wireless Communication System. *IEEE Commun. Lett.* **2021**, *25*, 3699–3703. [CrossRef]
15. Zeng, P.; Qiao, D.; Wu, Q.; Wu, Y. Active IRS aided WPCNs: A new paradigm towards higher efficiency and wider coverage. *arXiv* **2021**, arXiv:2111.11600.
16. Xu, D.; Yu, X.; Ng, D.W.K.; Schober, R. Resource Allocation for Active IRS-Assisted Multiuser Communication Systems. In Proceedings of the 2021 55th Asilomar Conference on Signals, Systems, and Computers 2021, Pacific Grove, CA, USA, 31 October–3 November 2021; pp. 113–119. [CrossRef]
17. You, C.; Zhang, R. Wireless communication aided by intelligent reflecting surface: Active or passive? *IEEE Wirel. Commun. Lett.* **2021**, *10*, 2659–2663. [CrossRef]
18. Liu, K.; Zhang, Z.; Dai, L.; Xu, S.; Yang, F. Active reconfigurable intelligent surface: Fully-connected or sub-connected? *IEEE Commun. Lett.* **2021**, *26*, 167–171. [CrossRef]
19. Dai, L.; Wang, B.; Wang, M.; Yang, X.; Tan, J.; Bi, S.; Xu, S.; Yang, F.; Chen, Z.; Di Renzo, M.; et al. Reconfigurable intelligent surface-based wireless communications: Antenna design, prototyping, and Experimental Results. *IEEE Access* **2020**, *8*, 45913–45923. [CrossRef]
20. Zhang, L.; Pan, C.; Wang, Y.; Ren, H.; Wang, K.; Nallanathan, A. Robust Beamforming Optimization for Intelligent Reflecting Surface Aided Cognitive Radio Networks. In Proceedings of the GLOBECOM 2020–2020 IEEE Global Communications Conference, Taipei, Taiwan, 7–11 December 2020; pp. 1–6. [CrossRef]
21. Xiao, H.; Dong, L.; Wang, W. Intelligent Reflecting Surface-Assisted Secure Multi-Input Single-Output Cognitive Radio Transmission. *Sensors* **2020**, *20*, 3480. [CrossRef]
22. Guan, X.; Wu, Q.; Zhang, R. Intelligent reflecting surface assisted secrecy communication: Is artificial noise helpful or not? *IEEE Wirel. Commun. Lett.* **2020**, *9*, 778–782. [CrossRef]
23. Abdullah, Z.; Chen, G.; Lambotharan, S.; Chambers, J.A. A Hybrid Relay and Intelligent Reflecting Surface Network and Its Ergodic Performance Analysis. *IEEE Wirel. Commun. Lett.* **2020**, *9*, 1653–1657. [CrossRef]
24. Wu, Q.; Zhang, R. Weighted Sum Power Maximization for Intelligent Reflecting Surface Aided SWIPT. *IEEE Wirel. Commun. Lett.* **2020**, *9*, 586–590. [CrossRef]
25. Gashtasbi, A.; da Silva, M.M.; Dinis, R.; Guerreiro, J. On the Performance of LDPC-Coded Large Intelligent Antenna System. *Appl. Sci.* **2023**, *13*, 4738. [CrossRef]
26. Gashtasbi, A.; da Silva, M.M.; Dinis, R. IRS, LIS, and Radio Stripes-Aided Wireless Communications: A Tutorial. *Appl. Sci.* **2022**, *12*, 12696. [CrossRef]
27. Alhamad, R.I. Intelligent Reflecting Surfaces with Adaptive Transmit Power and Energy Harvesting for Cognitive Radio Networks. *Wirel. Pers. Commun.* **2023**, *128*, 1003–1017. [CrossRef]
28. Hu, B.; Liu, J.; Wu, W.; Sun, Z. Robust secrecy rate maximization in IRS-assisted cognitive radio networks. *Phys. Commun.* **2022**, *55*, 101898. [CrossRef]
29. Son, P.N.; Duy, T.T.; Tuan, P.V.; Huynh, T.P. Short packet communication in underlay cognitive network assisted by an intelligent reflecting surface. *ETRI J.* **2023**, *45*, 28–44. [CrossRef]
30. Wright, S.J. Coordinate descent algorithms. *Math. Program.* **2015**, *151*, 3–34. [CrossRef]
31. Ma, W.-K.; Davidson, T.; Wong, K.M.; Luo, Z.-Q.; Ching, P.-C. Quasi-maximum-likelihood multiuser detection using semi-definite relaxation with application to synchronous CDMA. *IEEE Trans. Signal Process.* **2002**, *50*, 912–922. [CrossRef]
32. Jiang, H.; Zhang, Z.; Xiong, B.; Dang, J.; Wu, L.; Zhou, J. A 3D Stochastic Channel Model for 6G Wireless Double-IRS Cooperatively Assisted MIMO Communications. In Proceedings of the 2021 13th International Conference on Wireless Communications and Signal Processing (WCSP) 2021, Changsha, China, 20–22 October 2021; pp. 1–5. [CrossRef]
33. Jiang, H.; He, R.; Ruan, C.; Zhou, J.; Chang, D. Three-Dimensional Geometry-Based Stochastic Channel Modeling for Intelligent Reflecting Surface-Assisted UAV MIMO Communications. *IEEE Wirel. Commun. Lett.* **2021**, *10*, 2727–2731. [CrossRef]
34. Boyd, S.; Vandenberghe, L. *Convex Optimization*; Cambridge University Press: Cambridge, UK, 2004.